IEEE Access
Multidisciplinary ⋮ Rapid Review ⋮ Open Access Journal

Received 14 June 2024, accepted 12 July 2024, date of publication 16 July 2024, date of current version 24 July 2024.

Digital Object Identifier 10.1109/ACCESS.2024.3429181

RESEARCH ARTICLE

Optimized Sensorless Control of Five-Phase Permanent Magnet Synchronous Motor Using a Genetic Algorithm-Real Time Implementation

HAITHEM HAMAD BOUGHEZALA[1], KOUIDER LAROUSSI[1], SAAD KHADAR[1], AMEENA SAAD AL-SUMAITI[2], AND MAHMOUD A. MOSSA[3]

[1]Laboratory of Applied Automation and Industrial Diagnosis, Ziane Achour University, Djelfa 17000, Algeria
[2]Department of Electrical and Computer Engineering, Advanced Power and Energy Center, Khalifa University, Abu Dhabi, United Arab Emirates
[3]Electrical Engineering Department, Faculty of Engineering, Minia University, Minia 61111, Egypt

Corresponding authors: Haithem Hamad Boughezala (haithem.boughezala@univ-djelfa.dz) and Mahmoud A. Mossa (mahmoud_a_mossa@mu.edu.eg)

This work is supported by ASPIRE Virtual Research Institute (VRI) Program, Award Number VRI20-07.

ABSTRACT This paper presents an optimized backstepping control approach that combines a genetic algorithm (GA) and a robust sliding model observer (SMO) for achieving high-performance sensorless control of a 5-phase permanent magnet synchronous motor (5P-PMSM). Initially, a robust nonlinear strategy based on backstepping control is introduced to accurately track desired reference values of speed and direct-axis current. The stability analysis of the overall control system employs the Lyapunov theorem to ensure the convergence of tracking errors. However, the arbitrary selection of gains in backstepping control can impact controller quality. To address this, a novel numerical technique leveraging a genetic algorithm is proposed. This technique aims to determine optimal control gains while adhering to the physical limitations of the 5P-PMSM drive. Moreover, for sensor reduction purposes, a sliding model observer is devised to extract electromotive force information from the 5P-PMSM drive. Meanwhile, the angular position and motor speed are estimated using an adaptive back EMF observer. To validate the proposed solution, real-time modeling was implemented on an FPGA using the OPAL-RT 4500 simulator. The paper concludes by presenting real-time simulation results, illustrating the efficacy of the proposed approach across diverse test trajectories.

INDEX TERMS Backstepping control, 5P-PMSM drive, genetic algorithm, sliding model observer, OPAL-RT 4500 simulator.

I. INTRODUCTION

In recent years, the prominence of multiphase permanent magnet synchronous motors (PMSMs) has surged, surpassing other motor types like multiphase induction motors [1], [2]. This rise in popularity can be attributed to their remarkable attributes, which encompass high efficiency, low inertia, enhanced dynamic response, dependable operation, robustness, elevated power factor, compact size, straightforward structure, and reduced maintenance needs [3], [4], [5]. Consequently, multiphase PMSMs have emerged as prime contenders for real-world applications that necessitate superior performance, such as automobiles, household appliances, renewable energy systems, ship propulsion, robotics, aerospace applications, and more [1], [6], [7], [8]. Nevertheless, the inherent nonlinearity and multivariable nature of the 5-phase PMSM's dynamic model present formidable control challenges. These challenges arise from the intricate interplay between mechanical speed and electrical attributes, compounded by perturbations stemming from parameter variations [3], [6].

Conventional fixed-gain PI and PID controllers are often employed for the control of these machines [9], [10]. These controllers have found widespread use in practical

The associate editor coordinating the review of this manuscript and approving it for publication was Mou Chen.

applications due to their applicability and simplicity [10]. Within this paradigm, the PI controller performs admirably, yielding satisfactory outcomes. However, achieving optimal performance in the face of significant motor parameter uncertainties and mismatches induced by external disturbances becomes problematic [3], [11].

To tackle these issues, diverse nonlinear control methodologies have been proposed in the literature for PMSM control systems. These include input-output linearization control [12], sliding mode control [13], direct torque control [14], backstepping control [15], and more [2], [4], [5]. Yet, these control approaches are not without their own challenges and difficulties, including stability concerns, oscillations, chattering, and disturbances. Among the range of control techniques available, backstepping control stands out due to its robustness and superior dynamic performance [7]. However, the efficacy of this approach hinges on appropriately set control gains to achieve desired performance, including swifter dynamics in stator current and mechanical speed. The prevailing method for determining these gains involves empirical tuning, requiring a series of experiments to identify gain values that yield the desired performance. However, this approach often proves challenging and not consistently effective in producing optimal results. Consequently, the incorporation of stochastic search techniques such as genetic algorithms becomes essential to ascertain suitable gains. Prior research has indeed substantiated the effectiveness of such strategies in yielding optimal outcomes for optimal gain selection [16], [17].

Conversely, most control techniques typically necessitate accurate position and speed information to achieve high-performance variable-speed motor drives [2]. Conventionally, this information is acquired through speed sensors like resolvers, hall sensors, and encoders. However, the use of physical sensors introduces complexities and costs to the system, reducing its reliability and constraining its viability in harsh operating environments. Hence, sensorless control for PMSMs has gained traction as an effective and successful solution, relying on electromagnetic information to derive position and speed signals in lieu of mechanical sensors. In this context, a variety of sensorless methods have been proposed in literature to eliminate the need for speed sensors in three-phase PMSMs. These methods include model reference adaptive systems (MRAS) [18], Kalman filters (EKF) [19], sliding mode observers (SMO) [2], and approaches based on neural networks [20]. However, scant attention has been directed towards speed sensorless control for multiphase PMSMs. Notable exceptions include studies involving the MRAS estimator [3], EKF techniques [21], and SMO algorithms [11]. In [21], the author proposed a robust sensorless control strategy founded on an extended Kalman filter (EKF) for a 5P-PMSM drive. This observer design, despite accommodating motor parameter variations, exhibited satisfactory performance in terms of step reference speed. Nonetheless, the observer's complexity and high computational demands undermine its suitability for real-time applications. In [3], a different approach involved the development of a 5P-PMSM speed estimation technique utilizing a model reference adaptive system (MRAS) estimator for sensorless speed control. The MRAS estimator, distinguished by its heightened dynamic performance and precise estimation, does possess a notable limitation. It becomes sensitive to fluctuations in stator resistance, compromising its performance, especially in low-speed regions. The fault-tolerant fixed-time tracking control based on backstepping method presented in [22] was designed for a class of switched nonlinear systems with nonaffine faults. However, the designed control requires intensive calculations and proper initialization. Authors in [23] have used an output feedback tracking control of switched nonlinear systems with partially unstable subsystems, the performance tracking control is achieved using the Lyapunov theory. However, the used strategy is associated with high computational complexity, and the gains are sufficiently large to compensate the non-linearity present in the unstable subsystems. An alternative method, detailed in [11], introduced a nonlinear observer grounded in the sliding mode observer (SMO) principle. This approach targeted the estimation of back electromotive force (EMF), rotor position, and motor speed. SMO techniques exhibit superior dynamic behavior, simplicity, robustness, and reduced computational overhead. However, the key challenge of the SMO technique is the chattering phenomenon, arising from the discontinuity in the signum function [2], [5]. To address this, researchers have proposed substituting the signum function with a saturation or sigmoid function [11], which has demonstrated improved performance.

The proposed control scheme in this work offers a range of advantages that effectively mitigate the drawbacks outlined above. These benefits are succinctly summarized as follows:

Original Approach: This paper introduces an optimized backstepping control mechanism that employs a genetic algorithm for sensorless speed regulation in a 5P-PMSM drive. Notably, the entire control approach proposed in this work represents a novel solution that has not been previously explored by researchers;

Precise Gain Determination: A key advantage lies in the accurate determination of backstepping control gains, ensuring the attainment of desired performance benchmarks. Importantly, the algorithm put forth in this work stands out for its simplicity, contrasting with previous methodologies featured in [16] and [17];

Enhanced Sensorless Speed Regulation: The development of a straightforward sliding mode observer, grounded in the saturation function, contributes to sensorless speed regulation. This observer design effectively tackles chattering issues and maintains robustness in the face of load torque disturbances and parameter uncertainties, especially regarding stator resistance, stator inductance, and friction coefficient. The primary objective is to eradicate speed tracking errors, setting it apart from previous observer methods [2], [3], [5], [7], [11], [13], [18], [19], [20], [21];

Lyapunov Stability Analysis: The proposed scheme's overall system stability is rigorously analyzed using the Lyapunov theorem, thereby establishing its asymptotic stability;

Differentiated Sensorless Control: Distinguishing itself from earlier strategies, such as those presented in [18], [19], [20], and [21], the proposed sensorless control mechanism bypasses challenges associated with tuning time and computational complexity. This distinctive concept contributes a highly competitive solution for realizing high-performance control of multi-phase PMSM drives.

The paper is organized into seven distinct sections: Section II introduces the mathematical model of the 5P-PMSM, while Section III elaborates on the design of the backstepping strategy based on Lyapunov theory. In Section IV, a novel numerical technique employing a genetic algorithm is presented, followed by Section V, which details the design of a sliding model observer with phase loop lock. Real-time simulation results showcasing the effectiveness of the proposed control system are covered in Section VI, and finally, Section VII provides concluding insights that summarize the paper's contributions and significance.

II. MODELING OF FIVE-PHASE PMSM

Assuming that the magnetic field is sinusoidal, the magnetic flux is not saturated, and the impact of magnetic hysteresis in the PMSM system is negligible, the nonlinear model of 5P-PMSM drive can be established in a rotating reference frame (d_1-q_1, d_2-q_2) as [11], [21]:

$$\begin{cases} \dfrac{di_{d1}}{dt} = d_1 + \dfrac{V_{d1}}{L_s} \\ \dfrac{di_{q1}}{dt} = d_2 + \dfrac{V_{q1}}{L_s} \\ \dfrac{di_{d2}}{dt} = d_3 + \dfrac{V_{d2}}{L_{ls}} \\ \dfrac{di_{q2}}{dt} = d_4 + \dfrac{V_{q2}}{L_{ls}} \end{cases} \tag{1}$$

The electromagnetic torque and rotor speed are given by:

$$\begin{cases} T_{em} = K\varphi_f n_p i_{q1} \\ \dfrac{d\omega_r}{dt} = d_5 \end{cases} \tag{2}$$

where, i_{d1}, i_{q1}, i_{d2}, i_{q2} and V_{d1}, V_{q1}, V_{d2}, V_{q2} are the currents and voltages of stator winding. L_s and L_{ls} are the stator inductances. T_{em} and ω_r are the electromagnetic torque and mechanical speed. φ_f and n_p are the magnet flux and pair poles. Also, The parameters used in the system (1) and (2) are given as follows:

$$\begin{cases} d_1 = -\dfrac{R_s}{L_s} i_{d1} + \omega_r i_{q1} \\ d_2 = -\dfrac{R_s}{L_s} i_{q1} - \omega_r i_{d1} - \dfrac{\varphi_f}{L_s}\omega_r \\ d_3 = -\dfrac{R_s}{L_{ls}} i_{d2} + 3\omega_r i_{q2} \\ d_4 = -\dfrac{R_s}{L_{ls}} i_{q2} - 3\omega_r i_{d2} \\ d_5 = \dfrac{T_{em}}{J} - \dfrac{T_L}{J} - \dfrac{B\omega_r}{J} \end{cases} \tag{3}$$

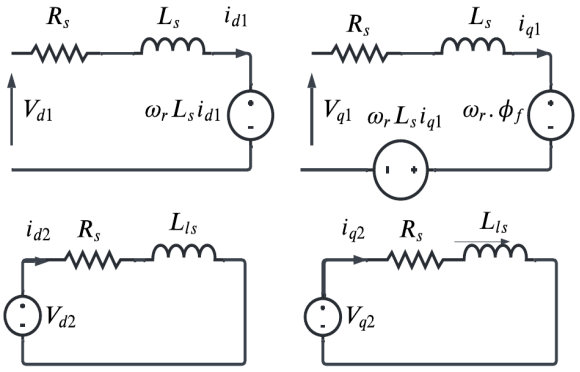

FIGURE 1. Equivalent circuit of 5P-PMSM drive.

TABLE 1. Parameters of 5P-PMSM drive.

Nominal data	Values
n_p	2
L_{ls}	0.13 mH
R_s	0.18 Ω
φ_f	0.163 Vs
J	0.11 Kg.m^2

where, R_s is the stator resistance. T_L is the load torque. J is the inertia moment. B denotes the friction coefficient. The equivalent circuit of 5P-PMSM drive is shown in Figure 1. The 5P-PMSM parameters are resumed in Table 1.

III. PROPOSED BACKSTEPPING CONTROL

The fundamental idea of backstepping control is to reduce the complicated nonlinear system to an equivalent form in order one cascade subsystems [19], [24], [25], [26], [27]. The Lyapunov approach offers stability. Figure 2 displays the block diagram of the proposed Backstepping strategy of 5P-PMSM drive. The objective of the introduced backstepping control is to attain accurate electrical speed tracking corresponding to the desired reference. The core principle underpinning backstepping control involves simplifying the intricate nonlinear system into a series of cascading equivalent first-order subsystems [19]. The outlined backstepping algorithm in this paper is devised in two distinct phases.

A. PHASE 1: CALCULATION OF REFERENCE CURRENTS

The speed controller should track the trajectory for input reference. Thus, the speed error with its derivative are presented as [11]:

$$\begin{cases} z_1 = \omega^* - \hat{\omega}_r \\ \dot{z}_1 = \dot{\omega}^* - \dot{\hat{\omega}}_r \end{cases} \tag{4}$$

The derivative of speed error can be established as:

$$\dot{z}_1 = \dot{\omega}^* - d_5 \tag{5}$$

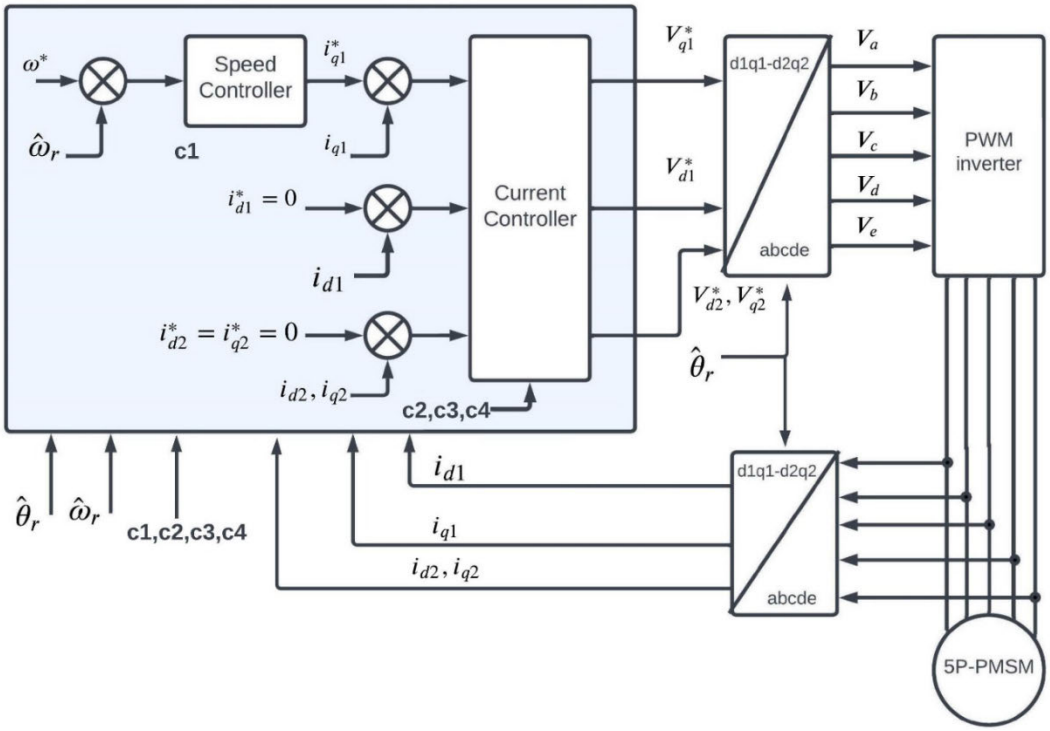

FIGURE 2. Block diagram of the suggested backstepping algorithm of 5P-PMSM drive.

The first Lyapunov function related with speed error is established to check the tracking performances as:

$$V_1 = \frac{1}{2} z_1^2 \tag{6}$$

Based on (5), the derivative of system (6) is computed as follows [25]:

$$\dot{V}_1 = z_1 \left(\dot{\omega}^* - d_5 \right) \tag{7}$$

Thus, the system (7) can be rewritten as:

$$\dot{V}_1 = z_1 \left(\dot{\omega}^* - d_5 \right) = -c_1 z_1^2 \tag{8}$$

where, $C_1 > 0$ and the derivative of speed error gives:

$$\dot{z}_1 = \dot{\omega}^* - \dot{\hat{\omega}}_r = -c_1 z_1 \tag{9}$$

The i_{q1} component contributes to developed torque, while the i_{d1}, i_{d2}, i_{q2} components contribute to the power losses [11]. Then the references currents can be described as [27]:

$$\begin{cases} i_{d1}^* = 0 \\ i_{q1}^* = \left(\dot{\omega}^* + \dfrac{T_L}{J} + \dfrac{B\hat{\omega}_r}{J} + c_1 z_1 \right) / \left(\dfrac{K \varphi_f n_p}{J} \right) \\ i_{d2}^* = 0 \\ i_{q2}^* = 0 \end{cases} \tag{10}$$

B. PHASE 2: CALCULATION OF REFERENCE VOLTAGES

The goal of this phase is to obtain the reference voltages based on the previous phase, where the current errors are obtained as [24]:

$$\begin{cases} z_2 = i_{d1}^* - i_{d1} \\ z_3 = i_{q1}^* - i_{q1} \\ z_4 = i_{d2}^* - i_{d2} \\ z_5 = i_{q2}^* - i_{q2} \end{cases} \tag{11}$$

Hence, their derivatives are expressed as follows:

$$\begin{cases} \dot{z}_2 = \dot{i}_{d1}^* - \dot{i}_{d1} \\ \dot{z}_3 = \dot{i}_{q1}^* - \dot{i}_{q1} \\ \dot{z}_4 = \dot{i}_{d2}^* - \dot{i}_{d2} \\ \dot{z}_5 = \dot{i}_{q2}^* - \dot{i}_{q2} \end{cases} \tag{12}$$

Using the system (10), the current errors are given as follows:

$$\begin{cases} z_2 = -i_{d1} \\ z_3 = \left(\dot{\omega}^* + \dfrac{T_L}{J} + \dfrac{B\hat{\omega}_r}{J} + c_1 z_1 \right) / \left(\dfrac{K \varphi_f n_p}{J} \right) - i_{q1} \\ z_4 = -i_{d2} \\ z_5 = -i_{q2} \end{cases} \tag{13}$$

Considering (13), the system (5) can be obtained as:

$$\dot{z}_1 = \frac{K \varphi_f n_p z_3}{J} - c_1 z_1 \tag{14}$$

Setting (1) in the system (12), one obtains:

$$\begin{cases} \dot{z}_2 = \dot{i}_{d1}^* - d_1 - \dfrac{V_{d1}}{L_s} \\ \dot{z}_3 = \dot{i}_{q1}^* - d_2 - \dfrac{V_{q1}}{L_s} \\ \dot{z}_4 = \dot{i}_{d2}^* - d_3 - \dfrac{V_{d2}}{L_{ls}} \\ \dot{z}_5 = \dot{i}_{q2}^* - d_4 - \dfrac{V_{q2}}{L_{ls}} \end{cases} \tag{15}$$

Therefore, to prove the overall stability of the studied control algorithm [11], a new Lyapunov function is defined as:

$$V_2 = \frac{z_1^2 + z_2^2 + z_3^2 + z_4^2 + z_5^2}{2} \tag{16}$$

It derivative of the system (16) becomes [25]:

$$\begin{aligned} \dot{V}_2 = & -c_1 z_1^2 - c_2 z_2^2 - c_3 z_3^2 - c_4 z_4^2 - c_4 z_5^2 \\ & + z_2 \left(c_2 z_2 + \dot{i}_{d1}^* - d_1 - \frac{V_{d1}}{L_s} \right) \\ & + z_3 \left(c_3 z_3 + K \varphi_f n_p z_1 + \dot{i}_{q1}^* - d_2 - \frac{V_{q1}}{L_s} \right) \\ & + z_4 \left(c_4 z_4 + \dot{i}_{d2}^* - d_3 - \frac{V_{d2}}{L_{ls}} \right) \\ & + z_5 \left(c_4 z_5 + \dot{i}_{q2}^* - d_4 - \frac{V_{q2}}{L_{ls}} \right) \end{aligned} \tag{17}$$

Consequently, if the variables within parentheses in the same expression are equal to zero, the derivative of the overall Lyapunov function (18) is negative.

$$\begin{cases} c_2 z_2 + \dot{i}_{d1}^* - d_1 - \dfrac{V_{d1}}{L_s} = 0 \\ c_3 z_3 + K \varphi_f n_p z_1 + \dot{i}_{q1}^* - d_2 - \dfrac{V_{q1}}{L_s} = 0 \\ c_4 z_4 + \dot{i}_{d2}^* - d_3 - \dfrac{V_{d2}}{L_{ls}} = 0 \\ c_4 z_5 + \dot{i}_{q2}^* - d_4 - \dfrac{V_{q2}}{L_{ls}} = 0 \end{cases} \tag{18}$$

The reference voltages are obtained as [11]:

$$\begin{cases} V_{d1}^* = L_s \left(c_2 z_2 + \dot{i}_{d1}^* - d_1 \right) \\ V_{q1}^* = L_s \left(c_3 z_3 + k \varphi_f n_p z_1 + \dot{i}_{q1}^* - d_2 \right) \\ V_{d2}^* = L_{ls} \left(c_4 z_4 + \dot{i}_{d2}^* - d_3 \right) \\ V_{q2}^* = L_{ls} \left(c_4 z_5 + \dot{i}_{q2}^* - d_4 \right) \end{cases} \tag{19}$$

Ultimately, the reference variables required to regulate the PMSM's speed have been determined by backstepping control. However, the effectiveness of this strategy depends on control gains that are adjusted suitably to produce the required performance, which includes faster dynamics in both motor speed and stator current. Therefore, a genetic algorithm is suggested in this work to determine the control gains of backstepping approach.

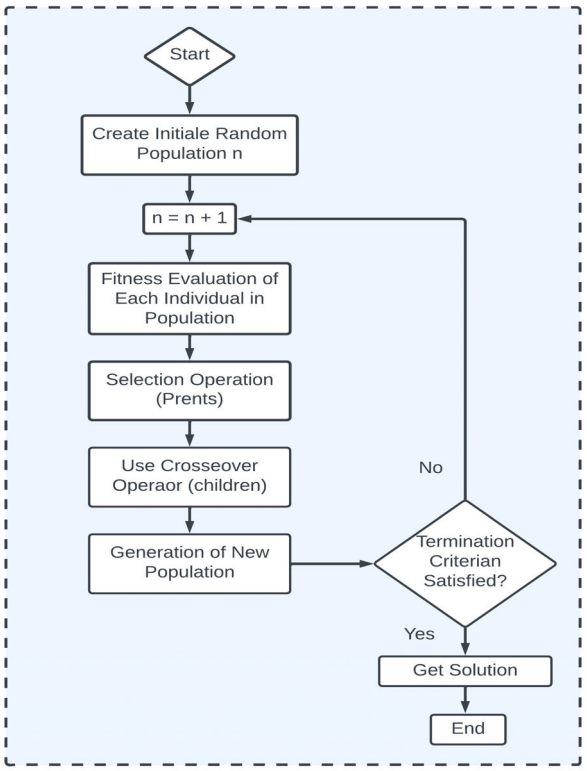

FIGURE 3. Flowchart of standard GA.

IV. ADOPTED GENETIC ALGORITHM

Genetic algorithms (GA) represent stochastic global search methods widely employed to address optimization challenges across various domains, including management, economics, and industry [16]. Figure 3 provides an overview of the flowchart detailing the genetic algorithm process. Generally, the GAs are presented based on three fundamental principles, as has been suggested by J. Holland:

- **The encoding:** operation of encoding parameters as genes and chromosome;
- **The operator of selection:** selection of the best suited and most efficient individuals;
- **The operators of reproduction:** crossover and mutation acting on genes.

Within the context of backstepping control, the pivotal challenge revolves around selecting appropriate control gains [19]. To surmount this hurdle, the integration of stochastic optimization techniques becomes imperative. Consequently, this work proposes the utilization of a genetic algorithm, which is implemented on the discrete model of the dynamical system equations. In our investigation, the proposed GAs are structured upon five fundamental steps:

1. Chromosome Design: Chromosomes are constructed using genes representing the control gains, as depicted in Figure 4.

The following constraints must be considered:

The Parameters (C_1, C_2, C_3, C_4) must remain within their predetermined intervals. Adherence to the physical

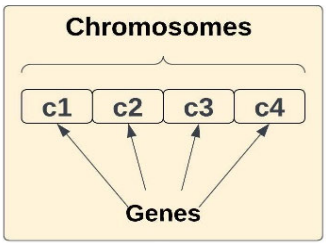

FIGURE 4. Chromosome structure.

TABLE 2. Selected optimized gains of backstepping controller.

$c1$	6000
$c2$	4000
$c3$	2500
$c4$	800

limitations of the 5P-PMSM drive is crucial, encompassing stator voltages, currents, and torque.

The objective function is formulated by encompassing various attributes indicative of desired performance. This incorporates time responses, overshoots, and dynamic errors pertaining to both the current and rotor speed of the 5P-PMSM drive. The fitness metric aggregates these attributes, with the genetic algorithm aiming to minimize them through the following equation:

$$\Gamma = \Delta\omega + \Delta i + \Delta T_{r\omega} + \Delta T_{ri} + D(\omega) + D(i) \tag{20}$$

where, $\Delta\omega$ and Δi are the relative errors of speed and current. $\Delta T_{r\omega}$ and ΔT_{ri} are the time response errors of speed and current. D(ω), D(i) are the overshoots of speed and current. The backstepping controller gains based on AG are selected in Table 2. The genetic algorithm parameters are resumed in Table 3.

2. Encoding: A decimal coding approach is adopted for its simplicity over binary coding. This is particularly apt given that control gains are represented as decimal values.

3. Selection Function: Employing a selection algorithm that combines the threshold and a two-competitor tournament mechanism alongside a selection probability P_s =0.8.

4. Genetic Operator: A linear discrete crossover operation is executed on parent chromosomes, yielding three potential offspring (F_1, F_2, F_3) as follows:

$$\begin{cases} F_1 = 0.5\,(P_1 + P_2) \\ F_2 = 1.5P_1 - 0.5P_2 \\ F_3 = -0.5P_1 + 1.5P_2 \end{cases} \tag{21}$$

Following the evaluation of these offspring and their verification for adhering to constraints, the superior two are selected and deemed descendants.

5. Mutation Operator: A Gaussian mutation is implemented, affecting a variable percentage of offspring and diminishing linearly from 30% to 0% at the end. Additionally, a constraint is imposed on the magnitude of mutation, with the magnitude decreasing as the number of generations progresses.

The pseudo code of of GA-Backstepping controller was written in the MATLAB and linked to the Backstepping controller from the Simulink platform. The pseudo-code of the proposed GA-Backstepping controller is presented as follows:

% Population Initialization
Identify the Population size (P = 20);
Define the parameters (C_1, C_2, C_3, C_4);
% GA options
Define the objective function
obj_fn = optimization_GAINS (C_1, C_2, C_3, C_4);
Select individuals based on their fitness values,
if the random individual value is less than the selected parents;
otherwise, return;
Perform crossover to generate new parents;
Apply the Backstepping parameters;
Perform mutation with certain probability;
Compare the new fitness values with the previous values;
% Cost function
Define the cost function
Cost_fn = optimization_ GAINS (C_1, C_2, C_3, C_4);
Combine the parameters of parents to produce a new generation;
Change randomly the value of (C_1, C_2, C_3, C_4);
Verify the performance criteria;
Condition verified;
end.

V. DESIGNED SLIDING MODE OBSERVER

In this section, a sliding model observer (SMO) is suggested to estimate the back-EMF and the 5P-PMSM speed as well as rotor position, where the stator voltages are considered measurable and taken as the observer inputs. The dynamic nonlinear model of the SMO can be constructed in the stationary reference frame ($\alpha 1$, $\beta 1$, $\alpha 1$, $\beta 1$) as follows [28]:

$$\begin{cases} L_s \dfrac{d\hat{i}_{\alpha 1}}{dt} = -R_s \hat{i}_{\alpha 1} + V_{\alpha 1} - K_1 sat\,(s_{\alpha 1}) \\ L_s \dfrac{d\hat{i}_{\beta 1}}{dt} = -R_s \hat{i}_{\beta 1} + V_{\beta 1} - K_1 sat\,(s_{\beta 1}) \\ L_{ls} \dfrac{d\hat{i}_{\alpha 2}}{dt} = -R_s \hat{i}_{\alpha 2} + V_{\alpha 2} - K_2 sat\,(s_{\alpha 2}) \\ L_{ls} \dfrac{d\hat{i}_{\beta 2}}{dt} = -R_s \hat{i}_{\beta 2} + V_{\beta 2} - K_2 sat\,(s_{\beta 2}) \end{cases} \tag{22}$$

where, K_1 and K_2 are the observer gains. Also, sat(s) is saturation function, which is expressed as [11]:

$$sat(s) = \begin{cases} 1 & if\ s \succ \chi \\ \dfrac{s}{\chi} & if\ |s| \leq \chi \\ -1 & if\ s \prec \chi \end{cases} \tag{23}$$

where, χ is positive constant. $S(X) = \left[s_{\alpha 1} \; s_{\beta 1} \; s_{\alpha 2} \; s_{\beta 2} \right]^T = \left[\hat{i}_{\alpha\beta} - i_{\alpha\beta} \right]^T$ is sliding surface. The stability of the SMO system based on the Lyapunov function is studied under two conditions, the first one is the Lyapunov function should be positive. While the second condition is the derivative of the sliding function is negative, which is selected as [28]:

$$H = \frac{1}{2} S(X)^T S(X) \tag{24}$$

Its derivative is written as:

$$\begin{aligned} \dot{H} &= \frac{1}{2} S(X)^T \dot{S}(X) \\ &= s_{\alpha 1}\dot{s}_{\alpha 1} + s_{\beta 1}\dot{s}_{\beta 1} + s_{\alpha 2}\dot{s}_{\alpha 2} + s_{\beta 2}\dot{s}_{\beta 2} < 0 \end{aligned} \tag{25}$$

Thus, the derivative of estimation error can be computed as:

$$\begin{cases} L_s \dfrac{ds_{\alpha 1}}{dt} = -R_s s_{\alpha 1} + e_{\alpha 1} - K_1 sat\left(s_{\alpha 1}\right) \\ L_s \dfrac{ds_{\beta 1}}{dt} = -R_s s_{\beta 1} + e_{\beta 1} - K_1 sat\left(s_{\beta 1}\right) \\ L_{ls} \dfrac{ds_{\alpha 2}}{dt} = -R_s s_{\alpha 2} + e_{\alpha 2} - K_2 sat\left(s_{\alpha 2}\right) \\ L_{ls} \dfrac{ds_{\beta 2}}{dt} = -R_s s_{\beta 2} + e_{\beta 2} - K_2 sat\left(s_{\beta 2}\right) \end{cases} \tag{26}$$

By carefully selecting the observer gains, the presented SMO can achieve the separation between observer design and state feedback. When the system arrives to the sliding surface.

$$\dot{S}(X) = S(X) = 0 \tag{27}$$

Substituting (27) into (26) yields:

$$\begin{cases} e_{\alpha 1} = K_1 sat\left(\hat{i}_{\alpha 1} - i_{\alpha 1}\right) \\ e_{\beta 1} = K_1 sat\left(\hat{i}_{\beta 1} - i_{\beta 1}\right) \\ e_{\alpha 2} = K_2 sat\left(\hat{i}_{\alpha 2} - i_{\alpha 2}\right) \\ e_{\beta 2} = K_2 sat\left(\hat{i}_{\beta 2} - i_{\beta 2}\right) \end{cases} \tag{28}$$

On the other hand, a simple algorithm of speed sensorless control is built to extract the back EMF value for good filtering so to estimate the 5P-PMSM speed, which can be written as follows [28]:

$$\begin{cases} \dfrac{d\tilde{e}_{\alpha 1}}{dt} = -\tilde{\omega}_r \hat{e}_{\beta 1} - \omega_r \tilde{e}_{\beta 1} - m\tilde{e}_{\alpha 1} \\ \dfrac{d\tilde{e}_{\beta 1}}{dt} = \tilde{\omega}_r \hat{e}_{\alpha 1} + \omega_r \tilde{e}_{\alpha 1} - m\tilde{e}_{\beta 1} \\ \dfrac{d\tilde{e}_{\alpha 2}}{dt} = -m_1 \tilde{e}_{\alpha 2} \\ \dfrac{d\tilde{e}_{\beta 2}}{dt} = -m_1 \tilde{e}_{\beta 2} \end{cases} \tag{29}$$

where, $\tilde{e}_{\alpha 1} = \hat{e}_{\alpha 1} - e_{\alpha 1}, \tilde{e}_{\beta 1} = \hat{e}_{\beta 1} - e_{\beta 1}, \tilde{e}_{\alpha 2} = \hat{e}_{\alpha 2} - e_{\alpha 2}, \tilde{e}_{\beta 2} = \hat{e}_{\beta 2} - e_{\beta 2}$ and $\tilde{\omega}_r = \hat{\omega}_r - \omega_r$.

Also, m, m_1 are constants that are obtained by applying the given stability conditions. Therefore, to demonstrate the stability of system (29), a new Lyapunov function is given as follows [11]:

$$H_1 = \frac{\tilde{e}_{\alpha 1}^2 + \tilde{e}_{\beta 1}^2 + \tilde{e}_{\alpha 2}^2 + \tilde{e}_{\beta 2}^2}{2} + \frac{\tilde{\omega}_r^2}{2\lambda} \tag{30}$$

TABLE 3. Genetic algorithm parameters.

GA parameters	Value
Population size	20
Number of genes	4
Selection Type	Threshold & Probabilistic Tournament
Mumber of generation	1000
Selection Probability	0.8
Crossover Type	Linear crossing (Wright)
Mutation rate	[0% , 30%]
Sampling frequency	0.0001s

TABLE 4. Constant gains of SMO algorithm.

K_1	K_2	$K_{P\omega}$	$K_{I\omega}$
700	300	25	0.15

Its derivative is written as:

$$\begin{aligned} \dot{H}_1 = {} & \dot{\tilde{e}}_{\alpha 1}\tilde{e}_{\alpha 1} + \dot{\tilde{e}}_{\beta 1}\tilde{e}_{\beta 1} + \dot{\tilde{e}}_{\alpha 2}\tilde{e}_{\alpha 2} \\ & + \dot{\tilde{e}}_{\beta 2}\tilde{e}_{\beta 2} + \frac{1}{\lambda}\tilde{\omega}_r\dot{\tilde{\omega}}_r \end{aligned} \tag{31}$$

where, $\lambda > 0$. Substituting (28) into (30) yields:

$$\begin{aligned} \dot{H}_1 = {} & -m\left(\tilde{e}_{\alpha 1}^2 + \tilde{e}_{\beta 1}^2\right) - m_1\left(\tilde{e}_{\alpha 2}^2 + \tilde{e}_{\beta 2}^2\right) \\ & + \tilde{\omega}_r\left(\hat{e}_{\alpha 1}\tilde{e}_{\beta 1} - \hat{e}_{\beta 1}\tilde{e}_{\alpha 1} + \frac{1}{\lambda}\dot{\hat{\omega}}_r\right) \end{aligned} \tag{32}$$

The function H_1 is positive. Thus, the first stability requirement is satisfied. The second requirement is that the derivative of the H_1 be smaller than zero. It is important for the $\dot{H}_1$ to be negative as:

$$\begin{cases} -m\left(\tilde{e}_{\alpha 1}^2 + \tilde{e}_{\beta 1}^2\right) - m_1\left(\tilde{e}_{\alpha 2}^2 + \tilde{e}_{\beta 2}^2\right) < 0 \\ \tilde{\omega}_r\left(\hat{e}_{\alpha 1}\tilde{e}_{\beta 1} - \hat{e}_{\beta 1}\tilde{e}_{\alpha 1} + \dfrac{1}{\lambda}\dot{\hat{\omega}}_r\right) = 0 \end{cases} \tag{33}$$

Based on the estimated back EMF value, the estimated 5P-PMSM speed as follows:

$$\hat{\omega}_r = \lambda \int \left(\tilde{e}_{\alpha 1}\hat{e}_{\beta 1} - \tilde{e}_{\beta 1}\hat{e}_{\alpha 1}\right)dt \tag{34}$$

Finally, the adaptation law based on PI controller is computed as [24]:

$$\begin{aligned} \hat{\omega}_r = {} & K_{P\omega}\left(\tilde{e}_{\alpha 1}\hat{e}_{\beta 1} - \tilde{e}_{\beta 1}\hat{e}_{\alpha 1}\right) \\ & + K_{I\omega}\int \left(\tilde{e}_{\alpha 1}\hat{e}_{\beta 1} - \tilde{e}_{\beta 1}\hat{e}_{\alpha 1}\right)dt \end{aligned} \tag{35}$$

$$\hat{\theta}_r = \arctan\left(\frac{\hat{e}_{\alpha 1}}{\hat{e}_{\beta 1}}\right) \tag{36}$$

where, $K_{p\omega}$ and $K_{i\omega}$ are the PI speed gains. The constant gains used in SMO are chosen in Table 4, which is used in the real time simulation tests.

The general structure of the suggested observer for 5P-PMSM drive is presented in Figure 6. As can be seen, the feedback currents $i_{\alpha 1}$, $i_{\beta 1}$, $i_{\alpha 2}$, $i_{\beta 2}$ and the stator voltage $V_{\alpha 1}$,

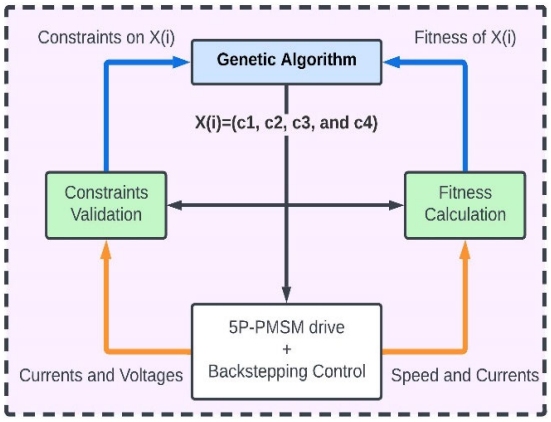

FIGURE 5. Block diagram of the gains determination algorithm.

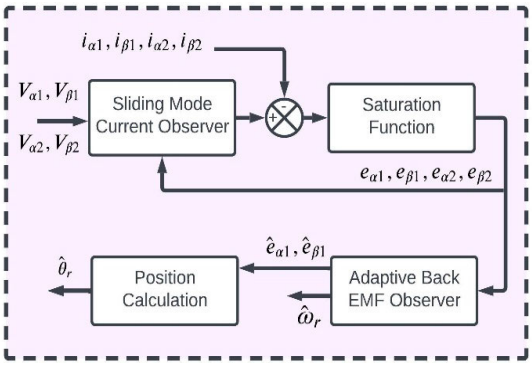

FIGURE 6. General structure of proposed observer for 5P-PMSM drive.

$V_{\beta1}$, $V_{\alpha2}$, $V_{\beta2}$ are the SMO inputs. While the estimated 5P-PMSM speed and rotor position are the outputs of the suggested observer.

VI. REAL-TIME SIMULATION RESULTS

The merits of the introduced backstepping technique, leveraging the genetic algorithm for a 5P-PMSM drive, along with the robustness and accuracy of the proposed sliding model observer, are rigorously substantiated through real-time simulations conducted on the OPAL-RT 4500 simulator.

A series of real-time simulations are executed to assess the performance of the suggested control strategy across diverse operational scenarios. These scenarios encompass load variations, alterations in motor parameters, and emulation of industrial test trajectories. The schematic illustration of the real-time setup utilizing the OPAL-RT 4500 simulator is visualized in Figure 7.

A. FIRST TEST: LOAD TORQUE CHANGE

The inaugural test serves to underscore the efficacy and performance of the proposed sensorless algorithm. In this evaluation, the estimated speed takes the place of the measured speed. The real-time outcomes of the sensorless control strategy, augmented by the AG with SMO system, are depicted in Figure 8.

The prescribed reference speed remains constant at 100 rad/s, while an applied load torque of 5 N.m is introduced at 0.5 s. The alignment between the actual speed and the estimated speed of the 5P-PMSM drive is presented in Figure 8(a). Evidently, the estimated speed adeptly shadows the actual speed in accordance with the imposed reference speed, devoid of any overshoot. This attests to the effectiveness of the proposed sensorless control solution. Figure 8(b) illustrates the speed tracking error between the actual speed and the estimated counterpart. This error remains minimal, hovering around 0.02 rad/s during the motor's steady-state operation. Notably, negligible error is observed during moments of load torque variation. Importantly, this speed tracking error showcases a significant reduction compared to errors encountered in prior works [3], [4], [5], [11], [15], [19], highlighting the precision and robust tracking dynamics introduced by the proposed SMO system.

Developed torque and applied load torque are visualized in Figure 8(c). The motor's torque dynamics post-load torque alteration are evidently swift and accurate. In steady-state operation, the motor torque aligns seamlessly with the imposed load torque, accompanied by acceptable ripples. These observations stand in contrast to findings in [6], [7], [14], [19], and [21].

Figure 8(d) illustrates the sinusoidal waveform of the five-phase currents within the 5P-PMSM drive. Notably, the currents exhibit balanced sinusoidal behavior, marked by a reduction in chattering—a notable improvement compared to previous instances of chattering observed [5], [11], [13]. Furthermore, figure 8(e) presents a comparison between the estimated rotor position, derived from the SMO system, and the real rotor position. Evidently, the rotor position maintains a periodic pattern oscillating between zero and 2π rad. Impressively, the estimated position aligns seamlessly with the real rotor position, underscoring the minimal rotor position error exhibited in Figure 8(f).

B. SECOND TEST: ROBUSTNESS TEST

A comprehensive robustness examination is undertaken to validate the proposed sensorless control's performance under low-speed operation. Specifically, a fixed step of 5 rad/s is introduced, coupled with an applied load torque of 5 N.m at 0.5 s. Of paramount importance is the investigation of the 5P-PMSM drive's response to parameter uncertainties. These uncertainties are delineated in Figure 9(a) and manifest as follows:

$$R_s = \begin{cases} 0.18\Omega & 0 < t < 0.2 \\ 0.27\Omega & 0.2 < t < 1, \end{cases}$$

$$L_s = \begin{cases} 2.1mH & 0 < t < 0.4 \\ 3.15mH & 0.4 < t < 1 \end{cases} \quad \text{and}$$

$$J = \begin{cases} 0.0011Kg.m^2 & 0 < t < 0.7 \\ 0.00165Kg.m^2 & 0.7 < t < 1 \end{cases}$$

FIGURE 7. The overall structure of the real-time setup.

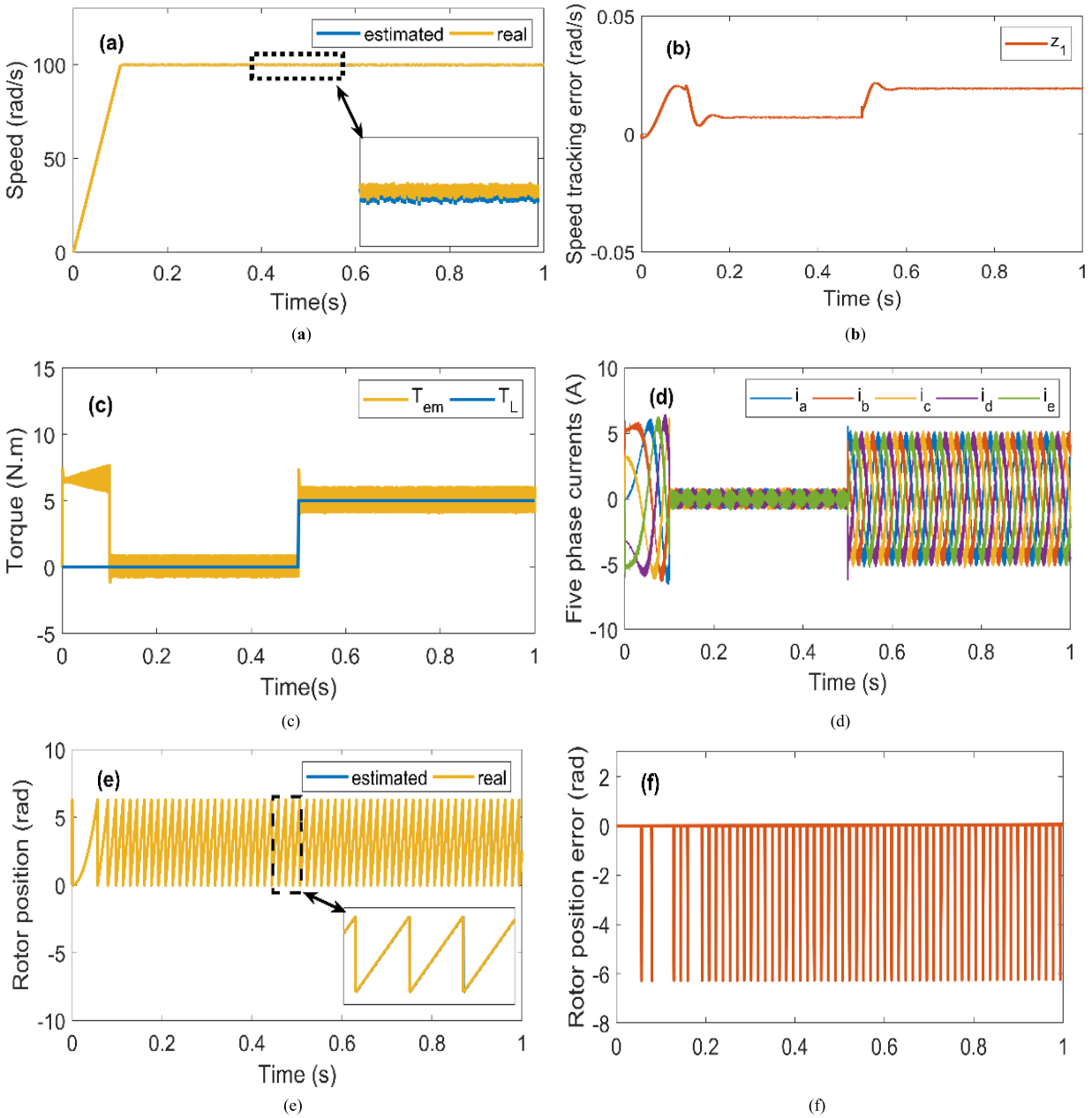

FIGURE 8. Results of real time simulation of suggested sensorless algorithm under load torque change: (a) Real speed and estimated speed; (b) Speed tracking error; (c) Developed torque and applied load torque; (d) Five-phase currents; (e) Real rotor position and estimated position signal; (f) Rotor position error.

This examination is instrumental in understanding the impact of motor parameter fluctuations on the proposed control algorithm. The real-time findings of the sensorless control strategy, underpinned by the AG with SMO system, amidst parameter uncertainties are portrayed in Figure 9.

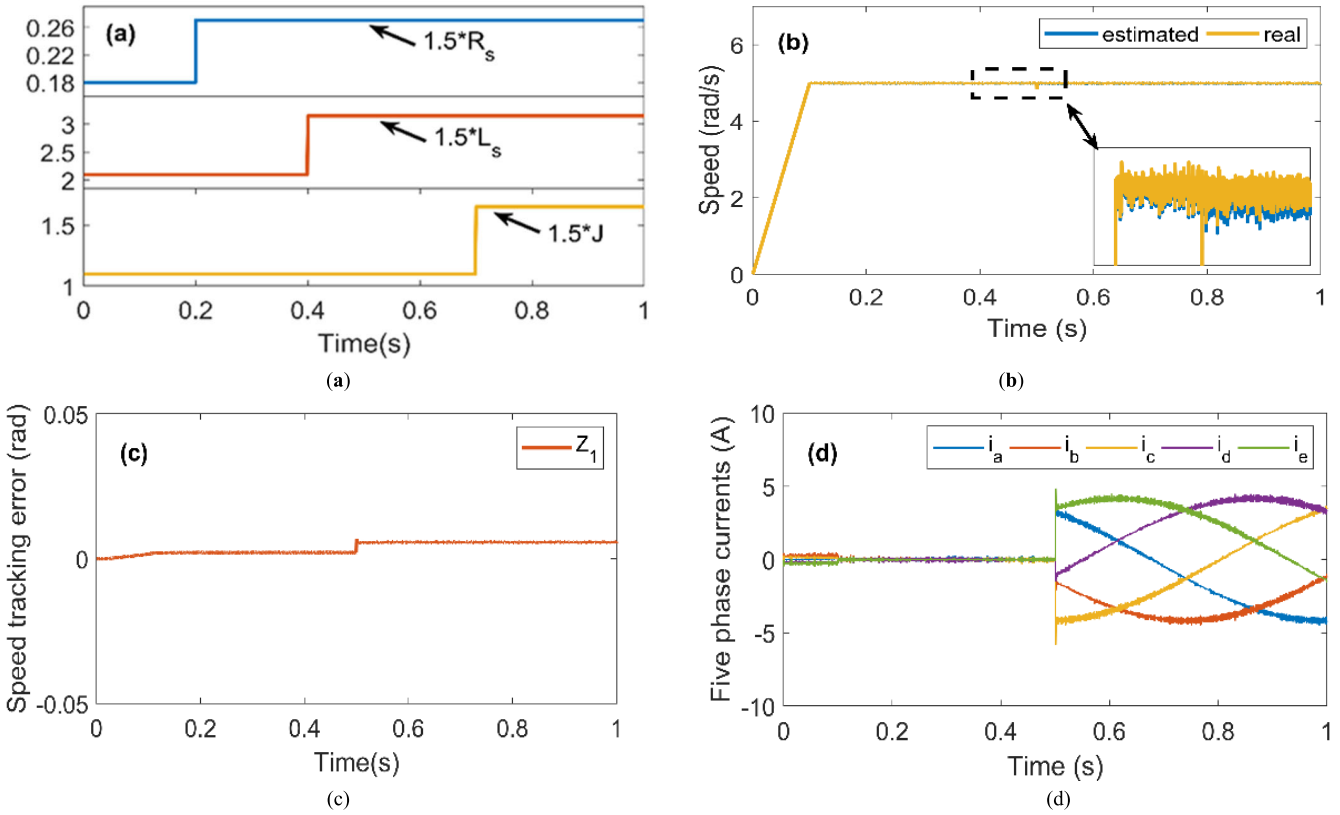

FIGURE 9. Results of real time simulation of suggested sensorless algorithm under parameter uncertainties at 5 rad/s: (a) Motor parameter variation of the 5P-PMSM drive; (b) Estimated speed and actual speed; (c) Speed tracking error; (d) Five-phase currents.

Figure 9(b) illustrates the measured real speed and the corresponding estimated speed at a low speed of 5 rad/s. The estimated speed tracks the actual speed with remarkable fidelity, even during low-speed operations devoid of any discernible overshoot. This behavior underscores the control algorithm's robustness and precision, even when subjected to low-speed conditions. Notably, the algorithm's performance remains resilient to changes in motor parameters—a contrast to findings in [2], [5], and [12].

The speed tracking error is impressively mitigated from 0.015rad/s to 0.008rad/s compared to previously reported results [2], [3], [4], [5], [11], [19], as depicted in Figure 9(c). This outcome serves as a testament to the sensorless control's superior performance, ensuring a stable operational mode for the 5P-PMSM drive, even during low-speed operation (within 5 rad/s). Figure 9(d) reveals the sinusoidal nature of the five-phase currents within the 5P-PMSM drive, observed even amidst motor parameter fluctuations and low-speed operation.

C. THIRD TEST: INDUSTRIAL TEST TRAJECTORIES

To ascertain the viability of the proposed sensorless algorithm, an industrial operating profile of the 5P-PMSM drive is employed, mirroring the profile provided in [7]. This profile is chosen due to its ability to encapsulate diverse scenarios across a broad spectrum of reference speed changes and load torque variations, rendering it a robust testbed for assessment. As illustrated in Figures 10(a) and 10(b), this profile traverses an array of distinct scenarios, offering a comprehensive evaluation of the sensorless algorithm's performance under realistic industrial conditions.

Figure 10(c) juxtaposes the measured real speed against the estimated counterpart. The convergence of estimated and actual speed profiles to the reference profile is conspicuous, manifesting minimal overshoot. Notably, the speed tracking error remains negligible across varying reference speeds and applied load torques, as evidenced in Figure 10(d). This underscores the sensorless algorithm's adeptness in delivering precise tracking dynamics and remarkable accuracy.

Figure 10(e) uncovers the amplitude behavior of the five-phase currents, resonating with the dynamic characteristics of the 5P-PMSM operation under diverse scenarios. Notably, during intervals when the motor speed reaches zero, the five-phase currents adopt DC-like characteristics. Furthermore, figure 10(f) reaffirms the efficacy of the proposed approach as the estimated rotor position aligns closely with the real signal, attesting to the algorithm's robustness and accuracy.

Response of five-phase PMSM under different controls are resumed in Table 5. Based on the real-time outcomes from the three preceding tests, it is evident that the devised backstepping approach, rooted in the genetic algorithm and SMO

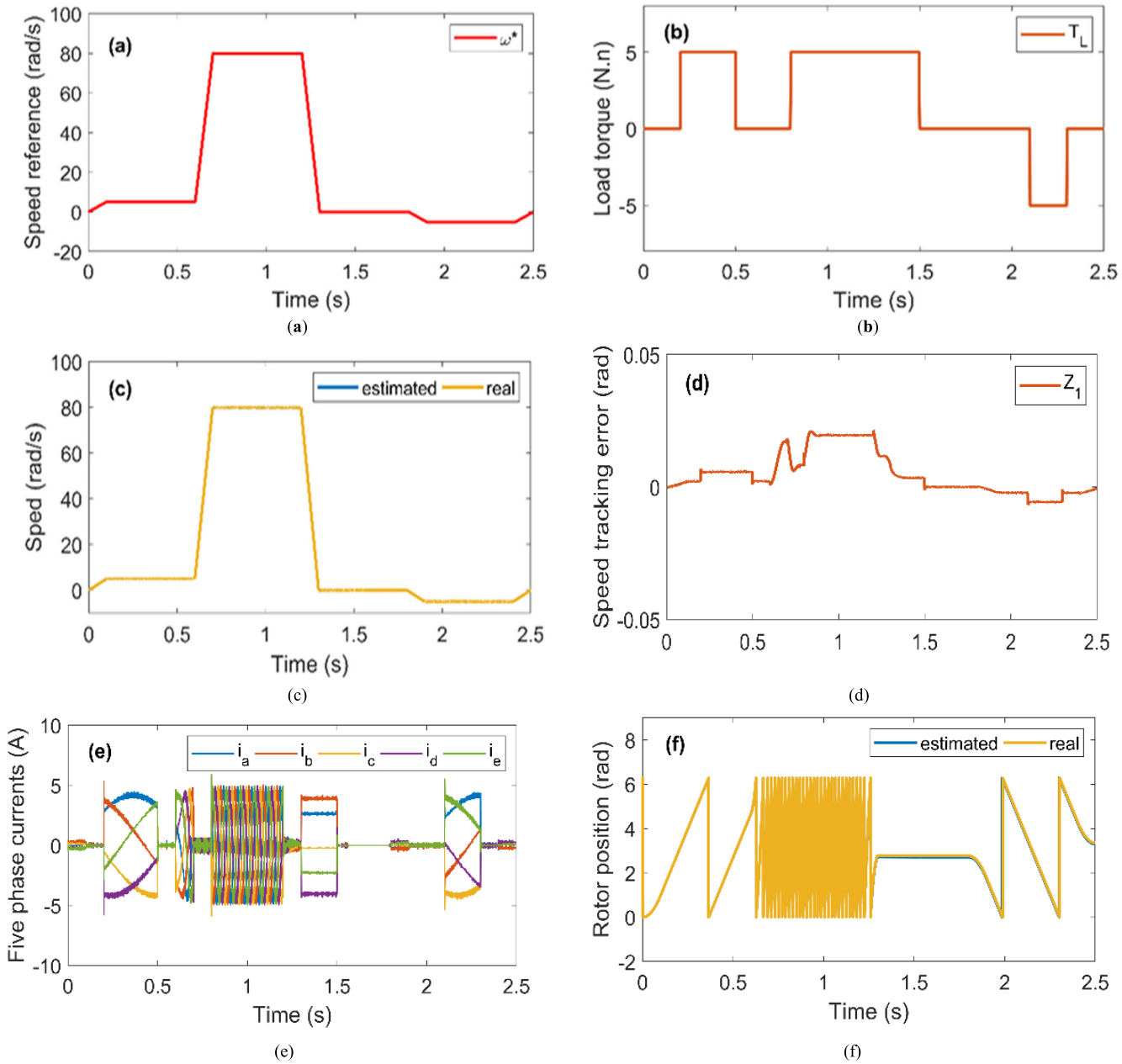

FIGURE 10. Results of real time simulation of suggested sensorless algorithm under industrial operation profile: (a) Speed reference; (b) Applied load torque; (c) Real speed and estimated speed; (d) Speed tracking error; (e) Five-phase currents; (f) Real rotor position and estimated position signal.

TABLE 5. Response of five-phase PMSM under different controls.

Works	Proposed Sensorless control based on a GA and a sliding model observer			Sensorless Vector Control Based on a Sliding Mode Observer [11]			Sensorless Backstepping Controller Using Extended Kalman Filter [19]		
Speed	Low speed	Rated speed	High speed	Low speed	Rated speed	High speed	Low speed	Rated speed	High speed
Rise Time	0.07	0.08	0.08	0.15	0.2	0.15	0.11	0.14	0.15
Settling Time	0.11	0.13	0.15	0.2	0.25	0.2	0.3	0.36	0.4
Speed Estimation Error	0.008	0.017	0.023	0.3	0.2	0.35	0.015	0.27	0.15

system, furnishes rapid response capabilities with heightened precision under varying load torque disturbances and reference speed changes. Simultaneously, the algorithm's robustness to motor parameter changes is evident, affirming its adaptability to real-world industrial applications. This distinctive blend of attributes positions the proposed

backstepping approach as a promising solution for 5P-PMSM drives across diverse industrial contexts.

VII. CONCLUSION

This study delved into the realm of robust nonlinear control for the enhancement of the performance of the studied 5P-PMSM drive. Leveraging the potency of a genetic algorithm, we devised a backstepping controller that showcased remarkable performance. Additionally, we seamlessly integrated a sliding mode observer into the framework to achieve real-time and accurate rotor position and speed estimations. Rigorous validation was attained through Lyapunov's criterion, substantiating the stability of both the proposed controller and observer. The efficacy of the developed sensorless control was rigorously examined through real-time simulations executed on the OPAL-RT 4500 simulator. These simulations underscored the resilience and potency of the proposed sensorless control approach for the 5P-PMSM drive, even under the influence of parameter uncertainties. Particularly noteworthy were the variations in stator resistance, friction coefficient, and stator inductance, which are pivotal aspects in the dynamic behavior of a 5P-PMSM drive system.

Further observation revealed that the proposed sensorless control framework exhibited impressive load torque disturbance rejection capabilities, outperforming previous approaches by exhibiting smaller speed tracking errors. Consequently, this solution stands as a robust and efficient sensorless technique primed for practical applications. In future research, our focus will shift towards conducting practical experiments to validate the proposed sensorless scheme for the 5P-PMSM drive system.

REFERENCES

[1] W. Wang, X. Chen, and J. Wang, "Motor/generator applications in electrified vehicle chassis—A survey," *IEEE Trans. Transport. Electrific.*, vol. 5, no. 3, pp. 584–601, Sep. 2019.

[2] L. Dhamo and A. Spahiu, "An Improved performance of sensorless PMSM drive control with sliding mode observer in low-speed operation," *Int. J. Eng. Trends Technol.*, vol. 4, no. 5, pp. 2205–2211, 2013.

[3] L. Guo and L. Parsa, "Model reference adaptive control of five-phase IPM motors based on neural network," *IEEE Trans. Ind. Electron.*, vol. 59, no. 3, pp. 1500–1508, Mar. 2012.

[4] R. Ramírez-Villalobos, L. T. Aguilar, and L. N. Coria, "Sensorless H_∞ speed-tracking synthesis for surface-mount permanent magnet synchronous motor," *ISA Trans.*, vol. 67, pp. 140–150, Mar. 2017.

[5] S. Khadar, M. E. Kobbi, M. Menzou, A. Senni, S. Zakaria, and H. Ahmed, "Mover position control of open-end stator winding integrated to wind power system using dSPACE 1103 control board," in *Proc. 1st Int. Conf. Renew. Solutions Ecosyst., Towards Sustain. Energy Transition (ICRSEtoSET)*, Djelfa, Algeria, May 2023, pp. 1–5, doi: 10.1109/icrsetoset56772.2023.10525329.

[6] F. Mekri, J.-F. Charpentier, and E. Semail, "An efficient control of a series connected two-synchronous motor 5-phase with non sinusoidal EMF supplied by a single 5-leg VSI: Experimental and theoretical investigations," *Electr. Power Syst. Res.*, vol. 92, pp. 11–19, Nov. 2012.

[7] M. A. Hamida, J. de Leon, and A. Glumineau, "Experimental sensorless control for IPMSM by using integral backstepping strategy and adaptive high gain observer," *Control Eng. Pract.*, vol. 59, pp. 64–76, Feb. 2017.

[8] P. Tang, Y. Dai, and Z. Li, "Unified predictive current control of PMSMs with parameter uncertainty," *Electronics*, vol. 8, no. 12, p. 1534, Dec. 2019.

[9] S. Khadar, H. Abu-Rub, and A. Kouzou, "Sensorless field-oriented control for open-end winding five-phase induction motor with parameters estimation," *IEEE Open J. Ind. Electron. Soc.*, vol. 2, pp. 266–279, 2021.

[10] L. Wang, K. Xiao, L. de Lillo, L. Empringham, and P. Wheeler, "PI controller relay auto-tuning using delay and phase margin in PMSM drives," *Chin. J. Aeronaut.*, vol. 27, no. 6, pp. 1527–1537, Dec. 2014.

[11] A. Hosseyni, R. Trabelsi, M. F. Mimouni, A. Iqbal, and R. Alammari, "Sensorless sliding mode observer for a five-phase permanent magnet synchronous motor drive," *ISA Trans.*, vol. 58, pp. 462–473, Sep. 2015.

[12] S. Rebouh, A. Kaddouri, R. Abdessemed, and A. Haddoun, "Nonlinear control by input–output linearization scheme for EV permanent magnet synchronous motor," in *Proc. IEEE Vehicle Power Propuls. Conf.*, Sep. 2007, pp. 185–190, doi: 10.1109/VPPC.2007.4544122.

[13] M. L. Corradini, G. Ippoliti, S. Longhi, and G. Orlando, "A quasi-sliding mode approach for robust control and speed estimation of PM synchronous motors," *IEEE Trans. Ind. Electron.*, vol. 59, no. 2, pp. 1096–1104, Feb. 2012.

[14] C. Xia, J. Zhao, Y. Yan, and T. Shi, "A novel direct torque control of matrix converter-fed PMSM drives using duty cycle control for torque ripple reduction," *IEEE Trans. Ind. Electron.*, vol. 61, no. 6, pp. 2700–2713, Jun. 2014.

[15] X. Liu, G. Zhang, L. Mei, and D. Wang, "Backstepping control with speed estimation of PMSM based on MRAS," *Autom. Control Comput. Sci.*, vol. 50, no. 2, pp. 116–123, Mar. 2016.

[16] S. Chaouch, L. Abdou, L. C. Alaoui, and S. Drid, "Optimized torque control via backstepping using genetic algorithm of induction motor," *Automatika*, vol. 57, no. 2, pp. 379–386, Jan. 2016.

[17] A. Marvi Moghadam and S. Balochian, "Design of combined sliding mode controller back stepping using genetic algorithm," *J. Eng.*, vol. 2013, pp. 1–6, Mar. 2013.

[18] H. M. Kojabadi and M. Ghribi, "MRAS-based adaptive speed estimator in PMSM drives," in *Proc. 9th IEEE Int. Workshop Adv. Motion Control*, Oct. 2006, pp. 569–572.

[19] A. Kirad, S. Groini, and Y. Soufi, "Improved sensorless backstepping controller using extended Kalman filter of a permanent magnet synchronous machine," *Bull. Electr. Eng. Informat.*, vol. 11, no. 2, pp. 658–671, Apr. 2022.

[20] G. Zhang, G. Wang, D. Xu, and N. Zhao, "ADALINE-network-based PLL for position sensorless interior permanent magnet synchronous motor drives," *IEEE Trans. Power Electron.*, vol. 31, no. 2, pp. 1450–1460, Feb. 2016.

[21] T. Kamel, D. Abdelkader, B. Said, S. Padmanaban, and A. Iqbal, "Extended Kalman filter based sliding mode control of parallel-connected two five-phase PMSM drive system," *Electronics*, vol. 7, no. 2, p. 14, Jan. 2018.

[22] D. Cui, C. K. Ahn, and Z. Xiang, "Fault-tolerant fuzzy observer-based fixed-time tracking control for nonlinear switched systems," *IEEE Trans. Fuzzy Syst.*, vol. 31, no. 12, pp. 4410–4420, Dec. 2023.

[23] D. Cui, C. K. Ahn, Y. Sun, and Z. Xiang, "Mode-dependent state observer-based prescribed performance control of switched systems," *IEEE Trans. Circuits Syst. II, Exp. Briefs*, early access, Feb. 27, 2024, doi: 10.1109/TCSII.2024.3370865.

[24] K. Saad, K. Abdellah, H. Ahmed, and A. Iqbal, "Investigation on SVM-backstepping sensorless control of five-phase open-end winding induction motor based on model reference adaptive system and parametser estimation," *Eng. Sci. Technol., Int. J.*, vol. 22, no. 4, pp. 1013–1026, Aug. 2019.

[25] R. Trabelsi, A. Khedher, M. Faouzi, and M. Faouzi, "An adaptive backstepping observer for on-line rotor resistance adaptation," *Int. J. Sci. Techn. Autom. Control Comput. Eng.*, vol. 4, no. 1, pp. 1246–1267, 2010.

[26] S. Khadar, A. Y. Abdelaziz, Z. M. S. Elbarbary, and M. A. Mossa, "An improved sensorless nonlinear control based on SC-MRAS estimator of open-end winding five-phase induction motor fed by dual NPC inverter: Hardware-in-the-loop implementation," *Machines*, vol. 11, no. 4, p. 469, Apr. 2023.

[27] M. Moutchou, A. Abbou, and H. Mahmoudi, "MRAS-based sensorless speed backstepping control for induction machine, using a flux sliding mode observer," *TURKISH J. Electr. Eng. Comput. Sci.*, vol. 23, pp. 187–200, Jan. 2015.

[28] A. Hosseyni, R. Trabelsi, P. Sanjeevikumar, A. Iqbal, and M. F. Mimouni, "Sensorless back stepping control for a five-phase permanent magnet synchronous motor drive based on sliding mode observer," in *Advances in Power Systems and Energy Management* (Lecture Notes in Electrical Engineering). Singapore: Springer, 2018, pp. 251–261.